Spring 2-2013

Remote Sensing of Surface Visibility from Space: A Look at the United States East Coast

Amy L. Kessner
University of Nebraska-Lincoln, agehring3@huskers.unl.edu

REMOTE SENSING OF SURFACE VISIBILITY FROM SPACE: A LOOK AT THE UNITED STATES EAST COAST

by

Amy L. Kessner

A THESIS

Presented to the Faculty of

The Graduate College at the University of Nebraska

In Partial Fulfillment of Requirements

For the Degree of Master of Science

Major: Earth and Atmospheric Sciences

Under the Supervision of Professor Jun Wang

Lincoln, Nebraska

February, 2013

REMOTE SENSING OF SURFACE VISIBILITY FROM SPACE: A LOOK AT THE UNITED STATES EAST COAST

Amy L. Kessner, M.S.

University of Nebraska, 2013

Advisor: Jun Wang

While important for the management of air quality, human health and transportation, surface visibility data currently are only available through ground-based measurements, such as the Automated Surface Observing System (ASOS), and therefore lack spatial coverage. In analogy to the recent work of using satellite-based aerosol optical depth (AOD) to derive surface dry aerosol mass concentration at continental-to-global scale for cloud-free conditions, this study evaluates the potential of AOD retrieved from the MODerate Resolution Imaging Spectroradiometer (MODIS) for deriving surface visibility. For this purpose of evaluation, the truncated and discrete visibility data from daily weather reports are not suitable and the ASOS-measured one-minute raw surface extinction coefficient (b_{ext}) values have to be used. Consequently, a method for quality control on the b_{ext} data is first developed to eliminate frequent problems such as extraneous points, poor calibration, and bad formatting, after which reliable b_{ext} data are obtained to estimate the surface visibility that can be considered as ground truth. Subsequent analysis of the AOD and b_{ext} relationship on the East Coast of the United States reveals their average linear correlation coefficient (R) of 0.61 for all 12 (2000-2011) years of data at 32 ASOS stations, with the highest R value in summer and the lowest in winter. Incorporating the Goddard Earth Observing System, Version 5 (GEOS-5) modeled vertical profile of aerosols into the derivation of visibility from AOD is

evaluated for five different methods that are commonly used in the estimate of dry aerosol mass from AOD. For three years of available GEOS-5 data, scaling the modeled surface b_{ext} with the ratio between MODIS AOD and the modeled AOD is found to produce the best overall estimate of surface visibility that correlates with ASOS-based visibility with an R of 0.72 and a small negative bias of -0.03 km^{-1}. This study is among the first to demonstrate the use of the MODIS aerosol product over land to derive surface visibility.

TABLE OF CONTENTS

LIST OF TABLES AND FIGURES

TABLES

FIGURES

1. Introduction

Visibility is the greatest horizontal distance at which it is just possible to observe and identify particular objects. Therefore, accurate measurement and forecast of atmospheric visibility is important for the safety of both aviation and ground transportation, as well as for aesthetic reasons. Visibility can be reduced by natural conditions, such as clouds and fog, and also by the presence of aerosols, which can be natural or anthropogenic. Since heavy concentrations of aerosol (also known as particulate matter, PM) at Earth's surface are a component of poor air quality, accurate measurement and forecast of horizontal visibility can be useful for health applications.

Clear sky visibility decreased globally, with the exception of Europe, between 1973 and 2007 (Wang et al., 2009). During the 1970's, an increase in sulfate aerosols from coal consumption was the dominant cause of haziness (visibility decrease) in the eastern U.S. (Husar et al., 1981). A study by Bäumer et al. (2008) of an aging air mass in Germany shows a distinct decrease of surface visibility along with an increase in both particulate matter (PM) and aerosol optical depth (AOD). Several studies have shown a relationship between distinct atmospheric aerosols and their individual contributions to horizontal visibility (e.g. Malm et al., 1994).

Prior to 1990, most measurements of surface visibility were made by a human observer and thus were largely subjective. However, by the early 1990's, the Automated Surface Observing System (ASOS) began to replace human observation in the United States at ~1000 airports (NOAA et al., 1998). Yet, with coverage restricted to U.S. airports, the ASOS measurements cannot produce a complete picture of surface visibility. Satellite observations, on the other hand, are global, and can be used to retrieve aerosol

properties. Additionally, with the implementation of automated visibility measurements from ASOS, the definition of visibility has been altered from a horizontal surface measurement to essentially a point measurement since ASOS does not consider the horizontal variation of aerosol beyond the path length of air (~1.0 m) that ASOS samples. This change is favorable for using satellite data to derive surface visibility because satellite data (such as AOD) often are columnar quantities at high spatial resolution, and similar to ASOS visibility, they are meant to be representative over a finite area (such as over 10x10 km^2, even though the ASOS-reported visibility can be larger than 10 km).

There have been many studies that characterize the relationship between AOD and surface PM (e.g., Hoff and Christopher, 2009). A global study by van Donkelaar et al. (2006) showed correlations between 0.58 and 0.69 for daily AOD compared to PM2.5 (PM having diameter $\leq$ 2.5 um) averaged between 10:00 a.m. and 12:00 p.m. Local Time for the United States. These correlations were improved globally to between 0.77 and 0.83 when a chemical transport model (CTM) was incorporated to account for the vertical distribution of aerosol (van Donkelaar et al., 2010). Other studies have shown significant correlation ($R > 0.6$) over portions of the United States, but also that the correlation varies by season (e.g., Wang and Christopher, 2003; Zhang et al., 2009; Green et al., 2009). This is because there are many factors that complicate the AOD-PM relationship such as aerosol size, aerosol type, diurnal variation, relative humidity, and the vertical structure of aerosol extinction (van Donkelaar et al., 2006, 2010; Gupta and Christopher, 2009a, 2009b). For example, the measurements of PM mass (for air quality applications) are usually taken in dry conditions (at temperature ~50°C, Watson et al., 1998; Allen et al., 1997), and hence do not take into account the ambient conditions of the atmosphere.

However, relative humidity (RH) can affect the size and water content of an aerosol, and thus the scattering and absorbing properties (Tang and Munkelwitz, 1994; Tsay et al., 1991; Wang et al., 2008). These factors can be partially overcome in the study of AOD-visibility relationship because AOD and visibility are both ambient optical quantities, affected by the same RH effect on particle extinction.

While there is a clearer relationship between AOD and visibility, few studies have attempted to use satellite-retrieved AOD to infer visibility. An early study by Kaufman and Fraser (1983) showed a strong correlation of 0.85 between AOD and inverse visibility (1/Visibility) at Dulles airport during 1980 while a weaker correlation of 0.51 was found during 1981. Vermote et al. (2002) established a relation between AOD and visibility to be used for Visible/Infrared Imager/Radiometer Suite (VIIRS) data onboard the National Polar-orbiting Operational Environmental Satellite System (NPOESS). This relation developed for VIIRS was then used by Retalis et al. (2010) to determine AOD from visibility data in Cyprus. Fei et al. (2006) used principal component regression to retrieve visibility data over water in coastal China from NOAA/AVHRR satellite data within two emitted-infrared bands. A more recent study by Hadjimitsis et al. (2010) used the darkest pixel atmospheric correction algorithm on Landsat-5 TM data in cooperation with radiative transfer calculations to produce a horizontal visibility product.

As discussed, past studies have greatly focused on remote sensing of PM. Studies focusing on remote sensing of visibility are far sparser, and none of these studies, to our knowledge, have used remotely sensed AOD in conjunction with modeled aerosol vertical profile to infer surface visibility. In this study, we first develop a method of quality control for ASOS one-minute visibility data. Next, we conduct remote sensing of

surface visibility on the East Coast of the United States in four parts: 1) a four-day case study of a high-AOD event on the East Coast, 2) a long-term study of AOD versus visibility data, 3) incorporation of the vertical profile of aerosol using modeled data through five methods, and 4) application of one method to the original East Coast high-AOD event case study.

2. Relating AOD, Visibility, and Surface PM

2.1 Visibility

Visibility is defined as the length of path in the atmosphere required to reduce the luminous flux in a collimated beam from an incandescent lamp, at a color temperature of 2700 K, to 5 percent of its original value (WMO, 2008). In order to define visibility mathematically, it is important to first define the visual contrast. The visual contrast can be defined as follows:

$$C \equiv \frac{I' - I}{I'} \tag{1}$$

where *I* is the radiant intensity of an object and *I'* is the brightness of the surroundings. If the assumption is made of single-scattered radiation along a finite horizontal path (*S*), then the radiative transfer equation (RTE) can be written as follows:

$$\frac{dI}{d(b_{ext}s)} = -I + J \tag{2}$$

where b_{ext} is the extinction coefficient and *J* is the scattering source function. Assuming a horizontally homogenous atmosphere b_{ext} and *J* become constant along the line-of-sight, and the above equation can be integrated to get:

$$I(S) = I(0)e^{-b_{ext}S} + (1 - e^{-b_{ext}S})J \tag{3}$$

where *I(0)* is the radiance of the scene as seen without any attenuation from the atmosphere, and *I(S)* is the brightness of the scene at an observer's distance *S*. If the object is a blackbody then *I(0)* = 0 when considering reflected radiation only. If the background has intensity *I* □*(0)*, then $I(S) = J$, and equation 1 can be written as:

$$C = \frac{I'(0)t}{I'(0)t + (1 - t)J} \tag{4}$$

where $t = e^{-b_{ext}S}$. Finally, if we assume the background intensity is constant with distance, then $I'(0) = J$, and the visual contrast becomes:

$$C = t = e^{-b_{ext}S}. \tag{5}$$

Solving for *S*, we can now define visibility (*V*) as:

$$V = \frac{1}{b_{ext}} \ln C\ . \tag{6}$$

Setting the visual contrast equal to two percent (0.02) gives Koschmieder's equation:

$$V = \frac{3.912}{b_{ext}}. \tag{7}$$

However, in this study the meteorological optical range (MOR) is used, and thus the visual contrast is set to 5% (0.05) giving the definition of visibility to be (WMO, 2008; NCDC, 2003):

$$V = \frac{3.0}{b_{ext}}. \tag{8}$$

2.2 Aerosol Optical Depth (AOD), Surface PM, and Visibility

AOD, PM, and visibility are physically related. AOD is defined as the integral of the aerosol extinction due to scattering and absorption:

$$AOD = \int_0^z b_{ext}(rh(z))\, dz\ . \tag{9}$$

where b_{ext} is the atmospheric aerosol extinction coefficient, *rh* is the relative humidity, and *z* is the altitude.

To relate PM to AOD many complicating factors are involved:

$$AOD = H \cdot \frac{3}{4} \cdot PM(z_{srf}) \cdot \frac{f(rh(z_{srf}))}{\rho} \cdot \frac{Q_{dry}}{r_{eff}}. \quad (10)$$

where $f(rh(z_{sfc}))$ is the relative humidity factor, Q_{dry} is the extinction efficiency under dry conditions, r_{eff} is the effective radius, ρ is the aerosol mass density, and $H = \int_0^z \frac{b_{ext}(rh(z))}{b_{ext}(rh(z_{sfc}))} dz$, the shape of aerosol extinction profile (Koelemeijer et al., 2006).

As described earlier, the Koschmieder equation defines visibility mathematically and when the visual contrast (C) is set to five percent (0.05), visibility can be defined as (WMO, 2008; NCDC, 2003):

$$V = \frac{3.0}{b_{ext}(rh(z_{sfc}))}. \quad (11)$$

Thus, the relationship between visibility and AOD can be defined as:

$$AOD = \frac{3.0}{V} \cdot H. \quad (12)$$

Comparing equation 12 with equation 10, the simplicity of the AOD-visibility relationship when compared with the AOD-PM relationship can be seen. Additionally, the shape of the aerosol extinction profile (H) is an important link between AOD and the surface parameters PM and visibility.

3. Data

3.1 MODerate Resolution Imaging Spectroradiometer (MODIS)

This study uses the MODIS level 2 AOD product collection 5.1 (MOD04_L2 and MYD04_L2) from both Terra (morning observations) and Aqua (afternoon observations). MODIS measures spectral radiances at the top of the atmosphere in a wide spectral range from 0.41-15 μm (Remer et al., 2005). Radiances in the 0.47-2.13 μm range are used for aerosol retrieval (Levy et al., 2007; Tanré et al., 1997). This wide spectral range allows MODIS to retrieve aerosol optical depth (AOD) with greater accuracy than previous satellite sensors (Tanré et al., 1996; Tanré et al., 1997). Furthermore, MODIS can retrieve parameters characterizing aerosol size, such as the effective radius of the aerosol (ocean only) and the fraction of optical depth attributable to fine mode aerosol, which can be used to separate anthropogenic aerosols from natural aerosols (Remer et al., 2005). The MODIS Deep Blue aerosol retrieval algorithm allows for accurate retrieval of aerosol signals from background with highly reflective surfaces, such as deserts, providing thorough global coverage (Hsu et al., 2006). However, this study uses AOD retrieved from MODIS Dark Target algorithm only since the main focus is over a dark land surface (Levy et al., 2007). Data are in 10 km nominal spatial resolution, and for the latitudes studied here there is approximately one retrieval (if cloud free) per day, per satellite. Valid ranges for AOD in the mid-visible are -0.05 to 5.0. During the retrieval process, quality assurance (QA) confidence flags with value between 0 (bad) and 3 (good) are assigned to the AOD retrieval (Remer et al., 2009). In this study, only AOD values with QA flag values of 2 or 3 are used.

3.2 The Goddard Earth Observing Systems Model, Version 5 (GOES-5)

The Goddard Earth Observing Systems Model, Version 5 (GEOS-5) is an Earth system modeling including an atmospheric general circulation model, a module for treatment of atmospheric aerosols, and a data assimilation system (Rienecker et al. 2008). This study uses results of the GEOS-5 model driven with meteorological analyses provided by the Modern-Era Retrospective Analysis for Research and Applications (MERRA, Rienecker et al. 2011) and incorporating an aerosol module based on the Goddard Chemistry, Aerosol, Radiation, and Transport (GOCART) model (Colarco et al. 2010), which simulates the distributions of dust, sulfate, carbonaceous, and sea salt aerosols. The model was run at a horizontal spatial resolution of 0.625° longitude x 0.5° latitude (approximately 50 km-sized grid cells) with 72 vertical levels for the period 2003 – 2006. Results incorporate assimilation of aerosol optical depth derived from MODIS observations (da Silva et al., 2012, manuscript in preparation). The aerosol assimilation impacts the overall loading of aerosols in the model, but not their partitioning between simulated species or vertical profile.

3.3 The Automated Surface Observing System (ASOS)

ASOS utilizes the Belfort Model 6220 Visibility Sensor to measure forward scattering in a small volume of ambient air. As many as three ASOS Visibility Sensors may be installed at any given station in order to provide more thorough coverage of an area (e.g. multiple runways) as well as provide back-up sensors in case the primary sensor fails. The transmitter contains a xenon flashtube that produces light in the ~300 nm to 1100 nm wavelengths (EG&G Electro-Optics, 1983). The receiver is located at ~45° angle from the transmitter and is used to detect the scattered xenon light. The

receiver contains an optical longpass filter that attenuates any wavelengths below 515 nm, and through intercomparison testing, the model 6220 was found to have the same response to aerosols as it would if the emitter were a 690 nm source (C. Greenblatt, Belfort Instrument, 2012, personal communication). However, the sensor was initially calibrated by operating it near an Optec Transmissometer (Molenar et al., 1992). The Optec Transmissometer is an instrument that measures the attenuation of light (both scattering and absorption) at 550 nm, defining the standard value for the extinction coefficient in relation to visibility (NOAA et al., 1998). Thus, the calibration of the ASOS visibility sensor measurement of forward scattering leads to the assumption:

$$b_{sca} = b_{ext}(550nm) \tag{13}$$

Where b_{sca} is the scattering coefficient and b_{ext} is the extinction coefficient at 550 nm. Errors may be introduced by this assumption by absorption in the atmosphere. However, for the U.S. East Coast the single scattering albedo is approximately 0.95, so these errors should be minimal (Takemura et al., 2002). Therefore, this study will refer to the output from the ASOS visibility sensor's measurement of forward scattering as the extinction coefficient measured at 550nm (b_{ext}).

The ASOS network consists of the National Weather Service (NWS) and Federal Aviation Association (FAA) sites. Visibility observations are made at a one-minute time resolution, but the standard product is reported hourly and at values of: M1/4SM, (less than ¼ statute mile), 1/4SM, 1/2SM, 3/4SM, 1SM, 1 1/4SM, 1 1/2SM, 1 3/4SM, 2SM, 2 1/2SM, 3SM, 4SM, 5SM, 6SM, 7SM, 8SM, 9SM and 10SM (1 SM = 1.60934 km). Any observation of visibility greater than 10 miles is truncated into the reportable value of 10SM. Typical values of visibility under light, moderate, and heavy aerosol conditions

are greater than 40 km (> 25 SM), 15-40 km (9 – 25 SM), and less than 15 km (< 9 SM), respectively. The coarse increments used for the hourly data are therefore unsuitable for our study as information under light and moderate aerosol conditions are binned up into a single bin (10 SM). Because of this limitation we employ the one-minute ASOS data, which are found online in the form of the National Climatic Data Center's Data Set 6405 and 6406 (NCDC's DSI-6405 and DSI-6406). These datasets contain raw meteorological measurements, such as temperature, pressure, wind, and visibility (in the form of b_{ext} [km^{-1}]), taken at one-minute intervals, and thus are more appropriate for the applications in this study. Thus, this study uses the one-minute ASOS data for the years 2000-2011. However, it is important to note that there are currently no quality controls in place for the one-minute ASOS data.

4. ASOS One-minute Data Quality Control Method and Results

4.1 Method

The stored ASOS one-minute extinction coefficient data do not undergo any quality control like the ASOS hourly data. Common problems with the ASOS one-minute data include unrealistic variability, poor calibration, and inconsistent formatting. A possible cause of inconsistent formatting is noise in the wires when data are being transmitted. Furthermore, spider webs have also been known to cause a problem in measurements of visibility using the ASOS sensor as they affect the attenuation of light being received by the visibility sensor. Hence, before they are used to evaluate the visibility derived from MODIS AOD, the 1-minute surface extinction data need to undergo quality control. Here, a quality control method based upon work done by Richards et al. (1996), the Interagency Monitoring of Protected Visual Environments (IMPROVE) nephelometer (an instrument that measures ambient light scattering, b_{scat}) protocol (Cismoski, 1994), and the accuracy of the Belfort Model 6220 Visibility Sensor (Crosby, 2003) is developed.

Since any ASOS station may contain between one and three visibility sensors, the quality control implemented in this study needs to apply to stations with single sensors as well as stations with multiple sensors (two or three). To ensure reliable and repeatable ASOS visibility data, we applied the following criteria to filter the ASOS 1-minute b_{ext} data. A particular ASOS b_{ext} observation was retained if:

1) $0.05\ km^{-1} < b_{ext} \leq 7.5\ km^{-1}$. The IMPROVE protocol flags b_{scat} data when they exceed 5.0 km^{-1}. To include more low visibility measurements, a cut-off value of

7.5 km^{-1} (¼ mile visibility) was selected for this study. Also, the ASOS one-minute data are truncated at 0.05 km^{-1}, so data of this value are excluded from this study.

2) *Relative Humidity ≤ 95%.* Relative humidity data are obtained from ASOS one-minute measurements. This quality control is an IMPROVE qualification, and was chosen for this study to eliminate data where fog or precipitation may be occurring.

3) *The difference between one b_{ext} measurement and a 3-minute running average of b_{ext} measurements ≤ 20%.* The 3-minute rolling average is computed by taking the average of ±1 minute of data for each data point. This quality control was implemented to eliminate unrealistic variability and extraneous points within the data.

Additionally, for multi-sensor sites we require:

4) *The difference between a 3-minute running average of any two visibility sensors ≤ 20%.* This quality control was implemented to eliminate poor calibration between sensors, as well as unrealistic variability that may exist in one sensor, but not the other(s). The value of 20% was chosen (a) because the Belfort visibility sensor has an accuracy of ±10% (Crosby, 2003), and (b) to obtain the data with highest quality as possible for the evaluation of our estimate of visibility from MODIS AOD.

4.2 Results of ASOS Quality Control

To demonstrate our quality control method, we select time series of visibility data for the Thurgood Marshall Baltimore/Washington International Airport (KBWI) during

11-13 August and 24-26 August 2005 (Fig. 1). These two time periods are selected not only to show the contrast between a period of poor visibility and a period of good visibility, but to demonstrate the effectiveness of multiple visibility sensors as well.

Low visibilities occurred during 11-13 August 2005 (Fig. 1a-f). A diurnal cycle in visibility can be seen with the peak during the early afternoon each day and then decreasing into the night hours. When comparing the ASOS visibility data before quality control (Fig. 1a-c) and after quality control (Fig. 1d-f), most of the data (95%) are retained during quality control. This shows that the ASOS visibility sensors at KBWI are in good agreement during this period, and thus the data quality is very high.

However, during 24-26 August 2005, a discernible difference can be seen between the ASOS visibility data before quality control (Fig. 1g-i) and after quality control (Fig. 1j-l) as only 69% of the data are retained during this period. This can be attributed to several factors: 1) the first visibility sensor reaching the truncation point (60 km or 0.05 km^{-1}), 2) a calibration difference between the first and second sensor, and 3) extraneous data points found in both sensors. Calibration differences between visibility sensors at a given ASOS station are, unfortunately, common. For this reason, during our long-term analysis only ASOS stations with 2 or 3 visibility sensors will be used.

To illustrate the effectiveness of our data quality control, the histograms of KBWI visibility data for 2005 before and after quality control are plotted (Fig. 2). Before quality control, a noticeable difference in the shape of the histograms for each visibility sensor can be seen. Sensor 1 has a high relative frequency of visibilities in the 60 km bin while sensor 2 has a low relative frequency of visibilities in the same bin. This implies that sensor 1 is calibrated to output higher visibilities than sensor 2, which agrees with the

time series shown in Fig. 1. After the data have undergone quality control, data with calibration differences greater than 20% have been removed. This results in the histograms becoming more consistent between the two sensors. During this process 34.0% of the ASOS visibility data are lost.

To further explore data loss due to our quality control, Table 1 lists the 32 ASOS stations within our study region and how much data is lost for each station for each quality control criteria for the year 2005. The station with the greatest data loss during this period is the Norfolk International Airport (KORF) with a loss of 99.9% of the data. This loss is contributed almost entirely to a calibration difference between the two sensors at this station. The station that retained the most data is the Ronald Reagan Washington National Airport (KDCA) with a loss of 32.7% of the data. For all stations a majority of data was lost during the 4th quality control criteria with an average of 52.2% data loss for 2 sensor stations and 73.7% data loss for 3 sensor stations. The fewest data were lost during the 3rd quality control criteria with an average of 1.2% data loss for all stations. Again, it is important to reiterate that our purpose here is to keep the data that are assured with our best information to be in the highest quality. This assurance can come with a steep cost of data loss but is necessary for the most accurate results in the following sections.

5. Derivation of Visibility from MODIS AOD

5.1 Method

The establishment of a quality control regime for the ASOS one-minute b_{ext} data allows these data to be used in the analysis of surface visibility versus AOD. In order to analyze these data, ASOS b_{ext} data are collocated with the MODIS AOD data. A temporal average of either ±30 or ±90 minutes from the MODIS overpass time is used for the ASOS one-minute data. In both the hourly (±30 minutes) and 3-hourly (±90 minutes) averages, at least 50% of the data must be retained after ASOS quality control is performed. A spatial average of 5x5 pixel (50 km x 50 km) is used for the MODIS AOD data (e.g. Ichoku et al., 2002). In order for a pixel to be considered in the averaging, it must be cloud-free. Furthermore, at least 5 out of 25 cloud-free pixels are required to perform the spatial averaging and all pixels must have a QA of 2 or 3.

5.2 A Case Study

A high-AOD event occurred over the East Coast of the United States during 11-14 August 2005 (Fig. 3). During this period, a high-pressure system moved from the Kentucky region to the Atlantic Ocean, transporting and suppressing removal of smoke and sulphate aerosols in this area. Very high values of AOD (shown by red/pink color) correspond with this high-pressure system throughout the 4-day period. Furthermore, a strong degradation in visibility (orange/red circles) can be seen with the increase of AOD.

Fig. 4a shows comparison of MODIS AOD (5x5 pixel spatial average) against ASOS b_{ext} (3-hour temporal average) from the first two days of the study. A correlation of 0.59 is found for all the data during this time period, and an averaged correlation of 0.92 is found between the bin-averages of AOD and b_{ext}. This method of binning is

similar to that of Wang and Christopher (2003) as well as Gupta et al. (2006), which found correlations of 0.98 and 0.96, respectively, for bin-averaged daily mean $PM_{2.5}$ and AOD. Both correlation values in Fig. 4a are statistically significant with $p < 0.0001$. The dashed line represents the linear regression for all data points while the solid black line represents the weighted linear regression based on binned data giving a regression line of Vis = 0.26 AOD + 0.11 for both binned and non-binned data.

Consequently, this equation is used to create a basic model for ambient visibility from MODIS AOD:

$$V = \frac{3.0}{0.26 \cdot AOD + 0.11}. \quad (14)$$

This model (equation 14) is then used to calculate ambient visibility from MODIS AOD for 13-14 August, 2005 and is compared to the visibility recorded by ASOS (Fig. 4b). A good correlation of 0.68 is found with a linear regression of $V_{ASOS}=1.21V_{MODIS}$ - 2.12. With this basic model, the mean bias in the estimate of surface visibility from AOD is -0.61 km, indicating that the model slightly underestimates visibility. Furthermore, it is important to note that the upper limit of this model is ~27km, and thus this model is only useful during periods of high aerosol loading and will not be useful during relatively good visibility days. This is understandable because: (1) MODIS AOD retrieval is more accurate for moderate and high AOD conditions, and (2) ASOS sensors have a detection limit for clean conditions in which they lack the accuracy to capture the change of b_{ext}. Nevertheless, since days with low visibility are of high interest in transportation and air quality management (visibility greater than 10 miles is truncated in daily weather reports), the results from this case analysis warrant the assessment of the feasibility of using long-term MODIS AOD data to derive surface visibility.

5.3 Long-term Analysis of AOD vs. Visibility

ASOS stations used in the long-term (2000-2011) analysis of AOD and visibility are shown in Fig. 5a, including 25 2-sensor stations and 7 3-sensor stations. Correlation coefficients of ASOS hourly-averaged b_{ext} data vs. a MODIS AOD 5x5 pixel average for the 32 stations are shown in Fig. 5b for all years of data. Circles outlined in red are insignificant according to the two-tailed t-statistic test ($p > 0.01$) or have 3 or fewer available collocated points. The maximum correlation is 0.93 at the Chicago Midway International Airport (KMDW) and the minimum significant correlation is 0.24 at the Rayleigh County Memorial Airport (KBKW). The reason for this large difference in correlation is uncertain, but may be attributable to a small number of collocated points for KMDW (N=7) and a poor correlation during the spring and fall for KBKW (R=0.19 and R=0.08, respectively). The mean of all statistically significant correlation coefficients is 0.61 and the median correlation value is 0.63 for all 12 years of data.

Seasonally, geographical distributions of correlation coefficients are also shown for spring (MAM, Fig. 5c), summer (JJA, Fig. 5d), fall (SON, Fig. 5e), and winter (DJF, Fig. 5f) for all 12 years of data. Summer shows the highest correlations with a mean and median of 0.69 for statistically significant data. Following summer is fall with a mean and median of 0.56. Spring has a mean of 0.55 and a median of 0.59 while winter has the lowest correlations with a mean of 0.53 and a median of 0.45.

To further explore the seasonal relationship between AOD and b_{ext}, monthly correlations are explored for the years 2000-2011 (Fig. 6). Once again, the highest correlations are found in the summer months with the highest value R=0.70 in July. The lowest correlations are in the winter months with the lowest correlation, R=0.30, in

November. Interestingly, there is a strong correlation (R=0.75) between the monthly R-values and the number of collocated points for that month. This behavior of monthly R-values and correlations with number of points has many possible reasons:

1) There are high correlations in the summer because both AOD and surface visibility have a larger signal range. While the absolute uncertainties for each dataset may be large, their relative uncertainties are smaller.
2) There are low correlations in winter because the relative uncertainties of both measurements are large.
3) In the winter months the PBL is often stable, suppressing aerosol mixing, and, regardless of the magnitudes of either AOD or visibility, the column measurement of b_{ext} is not a good representation of the surface measurement of b_{ext}, and
4) ASOS one-minute b_{ext} measurements truncate at 0.05 km^{-1}, which reduces the number of valid collocation points. This happens most often in winter.

5.4 Incorporation of GEOS-5 Modeled Aerosol Vertical Profile

As suggested above, one of the greatest challenges in using remote sensing technique to map geophysical parameters near the surface is to the treatment of the shape of the vertical profile for that quantity. While most of aerosol mass reside in the boundary layer near the surface, there are cases where aerosol is transported at elevation. Thus, knowing the vertical profile *a priori* can help to specify the column/surface relationship. Many past studies have incorporated vertical profile information from various sources

such as LIDAR (e.g., Engel-Cox et al., 2006; Schaap et al., 2009) and global models (e.g., Liu et al., 2004; van Donkelaar et al., 2006, 2010; Gupta et al., 2009a, 2009b) to relate the AOD to surface PM2.5. A similar strategy is applied here.

Five methods of modeling visibility from MODIS AOD are developed in this study. Four of these methods incorporate simulated data from the NASA GEOS-5 MERRA Aerosol Reanalysis, such as planetary boundary layer height (PBLH) and surface extinction. For each method, 3 years of summer data (JJA) are analyzed (2003-2004, 2006) and then one summer of data is used as a 'test' summer (2005). Only summer data are used in this next section as the long-term analysis results showed the best correlations between AOD and surface visibility during the summer months, and thus summer time is the most favorable to evaluate different methods. For comparison purposes, the basic method of applying regression equations between MODIS AOD and ASOS b_{ext} without any treatment of aerosol vertical profile will be called Method 0 (M0).

5.4.1 Method 1 – "AOD / PBLH"

When aerosols are well-mixed within the planetary boundary layer (PBL), it may be assumed that the AOD within the PBL will be representative of the extinction at the surface. Thus, the PBLH has been used in previous work (e.g., Tsai et al., 2011) to determine the surface b_{ext} for comparison with surface parameters. Under this context, the following equation is used as Method 1 (M1):

$$b_{ext} = \frac{MODIS\ AOD}{GEOS5\ PBLH}. \tag{15}$$

5.4.2. Method 2 – "AOD/PBLH + Rayleigh"

In an atmosphere free of aerosols, Rayleigh scattering, the scattering of visible light due to air molecules, is the predominant form of visibility impairment. To account for

the amount of Rayleigh scattering near the surface, a method from Bodhaine et al. (1999) was used. First, the scattering cross-section was calculated:

$$\sigma_{sca}(\times 10^{-28} cm^2) = \frac{1.0455996 - 341.29061\lambda^{-2} - 0.90230850\lambda^2}{1 + 0.0027059889\lambda^{-2} - 85.968563\lambda^2} \quad (16)$$

where $\lambda = 0.55$ μm. This equation is accurate to better than 0.002% when $\lambda = 0.55$ μm (Bodhaine et al., 1999). Then, Rayleigh scattering at the surface was calculated from the formula:

$$b_{Ray} = \sigma_{sca} \frac{A\rho_a}{m_a} \quad (17)$$

where A is Avogadro's number, ρ_a is the air density at the surface, and m_a is the mean molecular weight of dry air calculated from the formula:

$$m_a = 15.0556(CO_2) + 28.9595 \quad (18)$$

where CO_2 is the concentration of CO_2 in the atmosphere expressed in parts per volume (Bodhaine et al., 1999). In this study, the concentration of CO_2 was calculated by averaging the June, July, and August monthly average CO_2 concentration for the years 2003-2006 as recorded at Mauna Loa, Hawaii (Keeling et al., 2009). This value was found to be 0.00037923 ppv.

The amount of Rayleigh scattering is added to M1 to create the second method (M2):

$$b_{ext} = \frac{MODIS\ AOD}{GEOS5\ PBLH} + b_{Ray}. \quad (19)$$

5.4.3. Method 3 – "GEOS-5 Scalar Extinction"

The third method (M3) is based on a method used by Liu et al. (2004). In this method, the GEOS-5 model is used to develop a scalar to multiply the MODIS AOD in order to derive b_{ext}. First, the mixing ratio of five species of aerosol (dust, sea salt,

sulphate, black carbon, and organic carbon) is taken from GEOS-5 and then multiplied by the pressure thickness and the mass extinction efficiency of the aerosol in order to determine a simulated surface b_{ext} value. Then, the following equation is used to determine a simulated extinction coefficient value:

$$b_{ext} = \frac{GEOS5\ surface\ b_{ext}}{GEOS5\ AOD} \cdot MODIS\ AOD + b_{Ray}. \quad (20)$$

5.4.4. Method 4 – "Combined Method"

The fourth and final method (M4) is the most complicated method as it incorporates aspects of M1, M2, and M3. This method uses GEOS5 data to remove the b_{ext} above the PBLH and then divides the remaining b_{ext} by the PBLH:

$$b_{ext} = \frac{\frac{GEOS5\ AOD - GEOS5\ AOD_{above\ PBL}}{GEOS5\ AOD} \cdot MODIS\ AOD}{PBLH} + b_{Ray}. \quad (21)$$

5.4.5 Results

A Taylor Diagram is used to demonstrate the results for each method (Fig. 7). The Taylor Diagram, designed by Taylor (2001), is useful in interpreting model performance by providing a statistical summary including the correlation, root-mean-square-difference (RMSD), and standard deviation. In Fig. 7, six Taylor Diagrams are shown where the cosine of the angle represents the correlation, the radius of the circles centered at "Obs" represents the normalized RMSD, and the radius of the polar plot (both the x- and y-axis) represents the normalized standard deviation. The closer to the "Obs" point, the better the modeled result. Fig. 7a – 7e contains a Taylor Diagram for 22 stations for June, July, and August in 2003, 2004, and 2006 for M0 – M4, respectively. Stations with $p > 0.01$ and the number of collocated points ≤ 3 are not shown or included in the analysis (10 stations total).

Results are generally good for MODIS AOD-ASOS b_{ext} correlations (M0) during the summers of 2003, 2004, and 2006 with a mean correlation of 0.74 and a median correlation of 0.73. However, the normalized RMSD and normalized standard deviation for all 22 stations are greater than the optimal value of 1.0 (e.g., "Obs" point). M3 and M4 improve the mean correlation by 0.02 and 0.04, respectively, and they improve the median correlation by 0.05 and 0.05, respectively. M3 and M4 also show normalized RMSD and normalized standard deviation values much closer to "Obs" point for all 22 stations. M1 and M2 did not improve the mean correlation or the median correlation. It is important to note that none of the methods universally improved the correlation for all stations. Furthermore, the correlation does not change between M1 and M2, showing that Rayleigh scattering does not contribute enough to the overall extinction to affect the correlation. However, it is important to include the amount of extinction due to Rayleigh scattering in order to have a more complete, and improved, physical relationship between MODIS AOD and ASOS b_{ext}.

Fig. 7f shows the Taylor Diagram comparison for all 32 stations for all methods. As expected, M3 and M4 not only show the highest average correlation values (0.72 and 0.74, respectively), but they also show normalized RMSD values and normalized standard deviation values much closer to 1.0 compared to M0 – M2. The results between M3 and M4 are very similar, and thus further analysis is performed on M3 and M4 for the year 2005.

The correlation between MODIS AOD and ASOS b_{ext} (M0 method) for all stations is 0.71, and the linear regression is $b_{ext,ASOS} = 0.32\ b_{ext,\ M0} + 0.05$ (Fig. 8a). The mean bias is 0.17 km^{-1}. The correlation between the b_{ext} from M3 and ASOS b_{ext} for the same three

years is 0.72, and the linear regression is $b_{ext,ASOS}$ =0.71 $b_{ext, M3}$ + 0.07 (Fig. 8b). The mean bias is greatly improved for M3 compared to M0 and is equal to -0.03. Furthermore, M3 shows an improvement in correlation of 0.01 when compared to M0. The correlation between b_{ext} from M4 and ASOS b_{ext} for the same three years is 0.74, and the linear regression is $b_{ext,ASOS}$ =0.76 $b_{ext, M4}$ + 0.07 (Fig. 8c). The mean bias is also greatly improved when compared to M0 and is equal to -0.04.

The regression equations from Fig. 8a, 8b, and 8c are used to create three models to be tested in the year 2005. The first model (Mod0) is based on M0 and defines b_{ext} as:

$$b_{ext} = 0.32 \cdot MODIS\ AOD + 0.05. \tag{22}$$

The second model (Mod3) is based on M3 and defines b_{ext} as:

$$b_{ext} = 0.71 \cdot \frac{GEOS5\ surface\ b_{ext}}{GEOS5\ AOD} \cdot MODIS\ AOD + 0.07. \tag{23}$$

The third model (Mod4) is based on M4 and defines b_{ext} as:

$$b_{ext} = 0.76 \cdot \frac{\frac{GEOS5\ AOD - GEOS5\ AOD_{above\ PBL}}{GEOS5\ AOD} \cdot MODIS\ AOD}{PBLH} + 0.07. \tag{24}$$

Results for the year 2005 are shown in Fig. 8d-e. Mod0 resulted in a correlation of 0.65 with a linear regression of $b_{ext,ASOS}$ = 0.82 $b_{ext,Mod0}$ + 0.05 (Fig. 8d). Mod3 shows an improvement in both correlation and regression over M0 with a correlation of 0.69 and a linear regression of $b_{ext,ASOS}$ = 1.01 $b_{ext,Mod3}$ + 0.02 (Fig. 8e). The mean bias for both Mod0 and Mod3 is -0.02 km^{-1}, an improvement from M0 and M3. Mod4 shows an improvement in both correlation and regression over M0 as well with a correlation of 0.67 and a linear regression of $b_{ext,ASOS}$ = 0.94 $b_{ext,Mod4}$ + 0.03 (Fig. 8e). The mean bias for Mod4 is -0.01 km^{-1}.

Since the difference in correlation between Mod3 and Mod4 is trivial, it is the

improvement in linear regression (i.e., closer to 1:1) that is most important. Mod3 shows the most improvement in correlation and, especially, in linear regression when compared to Mod0 and Mod4, and thus this model is also used to determine visibility for the case study presented at the beginning of this section (Fig. 3). A visibility map for 11-14 August 2005 can be seen in Fig. 9. The correlation between ASOS visibility and Mod3 visibility for all four days of data is 0.68 (Fig. 10a). For comparison against Fig. 4b, the correlation between ASOS visibility and Mod3 visibility is also shown for just 13-14 August 2005 (Fig. 10b). This correlation is 0.71, which is an improvement of 0.03 over the basic model developed from 11-12 August, 2005 (equation 14). There is also an improvement in slope and intercept. Furthermore, it is important to note that the upper range of this model is ~43 km, showing a great improvement in model range when compared to the basic model developed from 11-12 August, 2005 (~27 km). However, the root mean square error (RMSE) and bias both increase for Mod3 visibility when compared to the results from equation 14, which may reflect that the optimal results from the climatology (3-year) analysis may not be optimal for the individual cases. Nevertheless, it appears that the model we established in the analysis of 3-years of the data is representative for the summer in our study region, and can be applied in future years, but could be improved upon in future studies.

6. Summary and Conclusions

Surface visibility has important implications for air quality, but current measurements of visibility lack spatial coverage. This study aims to discover the feasibility of using satellite retrievals of AOD to determine surface visibility. First, a quality control regime was developed for the ASOS one-minute extinction coefficient (b_{ext}) data. This regime includes four criteria that must be met by each data point, resulting in an average data loss of 66.9% for all 32 stations used in this study. This large quantity of data lost is justified by the assurance that only the data of the highest quality is retained and analyzed.

A case study of a high-AOD event over the East Coast of the United States was studied to determine the basic relationship between MODIS AOD and ASOS b_{ext}. Results show a decrease in visibility with an increase in AOD. Furthermore, a good correlation was found (0.68) and a slight negative bias was present (-0.61 km^{-1}) when comparing visibility derived from MODIS AOD to ASOS visibility.

Following the case study, a long-term analysis of 32 East Coast ASOS stations for the years 2000-2011 was performed, and an average correlation between MODIS AOD and ASOS b_{ext} of 0.61 was found for all stations. This analysis shows that the relationship between MODIS AOD and ASOS b_{ext} is greatest during the summer months and lowest during the winter months. The highest monthly correlation of 0.70 is found in July, while the lowest correlation of 0.30 is found in November. The good correlation during the summer months is likely due to a well-mixed PBL during the summer, and thus the column measurement of b_{ext} is a good representation of the surface measurement of b_{ext}.

Finally, data from the NASA GEOS-5 MERRA Aerosol Reanalysis were used to determine the vertical profile of aerosol in order to develop five methods for deriving visibility from MODIS AOD (M0-M4). These methods were compared with a basic method that uses regression between MODIS AOD to ASOS b_{ext}. The third and fourth methods (M3 and M4) were found to produce the best results. M3 scales the modeled surface extinction coefficient with the ratio between MODIS AOD and the modeled AOD, and M4 scales the modeled AOD in the PBL with the ratio between MODIS AOD and modeled AOD and divides by the height of the PBL. These methods, along with the basic MODIS AOD – ASOS b_{ext} correlation (M0), were used to develop 3 models to be tested for the summer of 2005 (Mod0, Mod3, and Mod4). The Mod3 correlation was 0.04 higher when compared with Mod0 for the summer of 2005. Both Mod0 and Mod3 had a very small negative bias (-0.02 km^{-1}), but the RMSE of Mod3 was slightly smaller (0.07) compared to that of Mod0 (0.08). Mod4 also showed a higher correlation when compared to Mod0, but not as high as Mod3. Furthermore, Mod3 had a regression line closer to the 1:1 line when compared to both Mod0 and Mod4. Thus, Mod3 was applied to the 11-14 August, 2005 case study to determine modeled visibility from MODIS AOD. Results were generally good with a correlation of 0.68 for all four days and a correlation of 0.71 for the last two days, an increase of 0.03 against the basic model of derived visibility from MODIS AOD. An increased positive bias was found when Mod3 was applied to the case study data.

Currently, there is a lack of spatial coverage of surface visibility measurements. Satellites have the capability of global spatial coverage on cloud-free days. This study showed a good relationship between remotely sensed AOD and surface visibility at

airports across the East Coast of the United States. This relationship can generally be improved with the incorporation of modeled aerosol vertical profile information. These results promote the possibility of global surface visibility measurements from remotely sensed AOD. However, this study focused on regions that are often located in or near cities, and thus have high levels of aerosol. Remote sensing of visibility will likely prove to be more difficult in regions and times (e.g. winter) where visibility is generally good due to the limitation that satellite remote sensing of aerosols is more challenging in low AOD conditions, especially over land. Interestingly, any visibility larger than 10 miles is truncated to 10 miles in the operational weather observation report. Hence, this study at least shows the potential of using satellite AOD to derive the surface visibility that can be comparable with operationally reported visibility from ground observations. But, further studies are needed to evaluate the method of this study with visibility date from regions that have low AOD such as the Interagency Monitoring of Protected Visual Environments (IMPROVE) sites that are located at national parks and wilderness areas. Another challenge to the derivation of surface visibility from remotely sensed AOD is the incorporation of the vertical profile of aerosol. Five possible methods were shown in this study. These methods can be improved by using model simulated aerosol vertical profile in conjunction with *in situ* data from instruments such as lidar.

ACKNOWLEDGEMENTS

I am very grateful for the support, advice, and help from my graduate advisor, Dr. Jun Wang. In addition, I would like to thank the following people at the University of Nebraska – Lincoln: the members of my committee: Dr. Robert Oglesby and Dr. Clinton Rowe for their support, our department chair: Dr. David Watkins for advice, our secretaries: Tina Gray and Janelle Gerry for their logistical support, and the members of Dr. Wang's research group for all of the help, encouragement, and friendship they gave to me. I would like to thank my mentor at NASA Goddard Space Flight Center: Dr. Robert Levy as well as other NASA scientists: Dr. Lorraine Remer, Dr. Peter Colarco, Shana Mattoo, and Leigh Munchak for their advisement and encouragement. I would like to give a special thanks to the employees of Belfort Instrument for their guidance and expertise. Finally, I would like to thank my family for their continual support through this process. This project was funded partially by the NASA Nebraska Space Grant Student Fellowship and Mini-Grant program (Kessner) as well as the NASA GSFC Graduate Student Summer Program and Senior Internship Program (Kessner). This research is also partially supported by the NASA Radiation Sciences Program (Wang). We thank the data services provided by the Goddard Earth Sciences Data Center and the National Climatic Data Center Online Climate Data Directory.

References

Allen, G., C. Sloutas, P. Koutrakis, R. Reiss, F. W. Lurmann, and P.T. Roberts. 1997. "Evaluation of the TEOM Method for Measurement of Ambient Particulate Mass in Urban Areas." *J. Air & Waste Manage. Assoc.* 47 (6): 682-689.

Bäumer, D., B. Vogel, S. Versick, R. Rinke, O. Möhler, and M. Schnaiter. 2008. "Relationship of visibility, aerosol optical thickness and aerosol size distribution in an ageing air mass over South-West Germany." *Atmos. Environ*. 42 (5): 989-998. doi: 10.1016/j.atmosenv.2007.10.017.

Bodhaine, B. A., N. B. Wood, E. G. Dutton, and J. R. Slusser. 1999. "On Rayleigh Optical Depth Calculations." *J. Atmos. Ocean. Tech.* 16 (11): 1854-1861.

Colarco, P., A. da Silva, M. Chin, and T. Diehl. 2010. "Online simulations of global aerosol distributions in the NASA GEOS-4 model and comparisons to satellite and ground-based aerosol optical depth." *J. Geophys. Res.* 115 (D14): D14207. doi: 10.1029/2009JD012820.

Cismoski, D. S. 1994. *Nephelometer data reduction and validation (IMPROVE PROTOCOL)*. Fort Collins, CO: Air Resource Specialists, Inc.

Crosby, J. D. 2003. *Visibility Sensor Accuracy: What's Realistic?* Clarksville, Maryland: EnviroTech Sensors, Inc.

EG&G Electro-Optics. 1983. *High Efficiency Bulb Type Xenon Flashtubes and Lite-Pac Trigger Modules*. Salem, Mass.

Engel-Cox, J. A., R. M. Hoff, R. Rogers, F. Dimmick, A. C. Rush, J. J. Szykman, J. AL-Saadi, D. A. Chu, and E. R. Zell. 2006. "Integrating lidar and satellite optical depth with ambient monitoring for 3-dimensional particulate characterization." *Atmos. Environ.* 40 (40): 8056-8067.

Fei, H., W. Hong, Q. Junping, and W. Guofu. 2006. "Retrieval of Atmospheric Horizontal Visibility by Statistical Regression from NOAA/AVHRR Satellite Data." *J. Ocean Uni. China.* 5 (3): 207-212. doi: 10.1007/s11802-006-0003-4.

Green, M., S. Kondragunta, P. Ciren, and C. Xu. 2009. "Comparison of GOES and MODIS Aerosol Optical Depth (AOD) to Aerosol Robotic Network (AERONET) AOD and IMPROVE PM2.5 Mass at Bondville, Illinois." *J. Air & Waste Manage. Assoc.* 59 (9): 1082-1091. doi: 10.3155/1047-3289.59.9.1082.

Gupta, P., and S. A. Christopher. 2009. "Particulate matter air quality assessment using integrated surface, satellite, and meteorological products: Multiple regression approach." *J. Geophys. Res.* 114: D14205. doi: 10.1029/2008JD011496.

Gupta, P., and S. A. Christopher. 2009. "Particulate matter air quality assessment suing integrated surface, satellite, and meteorological product: 2. A neural network approach." *J. Geophys. Res.* 114: D20205. doi: 10.1029/2008JD011497.

Gupta, P., S. A. Christopher, J. Wang, R. Gehrig, Y. Lee, and N. Kumar. 2006. "Satellite remote sensing of particulate matter and air quality assessment over global cities." *Atmos. Environ.* 40 (30): 5880-5892. doi: 10.1016/j.atmosenv.2006.03.016.

Hadjimitsis, D. G., C. Clayton, and L. Toulios. 2010. "Retrieving visibility values using satellite remote sensing data." *Phys. Chem. Earth* 35 (1): 121-124.

Hoff, R. M. and S. A. Christopher. 2009. "Remote Sensing of Particulate Pollution from Space: Have We Reached the Promised Land?" *J. Air & Waste Manage. Assoc.* 59 (6): 645-675. doi: 10.3155/1047-3289.59.6.645.

Hsu, C. N., S-. C. Tsay, M. D. King, and J. R. Herman. 2006. "Deep blue retrievals of Asian aerosol properties during ACE-Asia." *IEEE Trans. Geosci. Remote Sens*. 44 (11): 3180-3195.

Husar, R. B., J. M. Holloway, D. E. Patterson, and W. E. Wilson. 1981. "Spatial and Temporal Pattern of Eastern U. S. Haziness: A Summary." *Atmos. Environ.* 15 (10): 1919-1928.

Ichoku, C., D. A. Chu, S. Mattoo, Y. J. Kaufman, L. A. Remer, D. Tanré, I. Slutsker, and B. N. Holben. 2002. "A spatio-temporal approach for global validation and analysis of MODIS aerosol products." *Geophys. Res. Lett.* 29 (12): 8006. doi: 10.1029/2001GL013206.

Kaufman, Y. J., and R. S. Fraser. 1983. "Light Extinction by Aerosols during Summer Air Pollution." *J. Climate Appl. Meteor.* 22: 1694-1706.

Keeling, R. F., S. C. Piper, A. F. Bollenbacher and J. S. Walker. 2009. Atmospheric CO_2 records from sites in the SIO air sampling network. In Trends: A Compendium of Data on Global Change. Carbon Dioxide Information Analysis Center, Oak Ridge National Laboratory, U.S. Department of Energy, Oak Ridge, Tenn., U.S.A. doi: 10.3334/CDIAC/atg.035.

Koelemeijer, R. B. A., C. D. Homan, and J. Matthijsen. 2006. "Comparison of spatial and temporal variations of aerosol optical thickness and particulate matter over Europe." *Atmos. Environ.* 40: 5304-5315. doi: 10.1016/j.atmosenv.2006.04.044.

Levy, R.C., L. A. Remer, S. Mattoo, E. F. Vermote, and Y. J. Kaufman. 2007. "Second-generation operational algorithm: Retrieval of aerosol properties over land from inversion of Moderate Resolution Imaging Spectroradiometer spectral reflectance." *J. Geophys. Res.* 112: D13211. doi:10.1029/2006JD007811.

Liu, Y., R. J. Park, D. J. Jacob, Q. Li, V. Kilaru, and J. A. Sarnat. 2004. "Mapping annual mean ground-level $PM_{2.5}$ concentrations using Multiangle Imaging Spectroradiometer aerosol optical thickness over the contiguous United States." *J. Geophys. Res.* 109: D22206. doi:10.1029/2004JD005025

Malm, W. C., K. A. Gebhart, J. Molenar, T. Cahill, R. Eldred, and D. Huffman. 1994. "Examining the relationship between atmospheric aerosols and light extinction at Mount Rainier and North Cascades National Parks." *Atmos. Environ.* 28 (2): 347-360.

Molenar, J. V., D. S. Cismoski, and R. M. Tree. 1992. *Intercomparison of Ambient Optical Monitoring Techniques.* Fort Collins, Colorado: Air Resource Specialists, Inc.

National Climatic Data Center. 2003. *Data Documentation for Data Set 3285 (DSI-3285): ASOS Surface 1 Minute Data*. Asheville, NC.

National Oceanic and Atmospheric Administration, Department of Defense, Federal Aviation Administration, and United States Navy. 1998: *Automated Surface Observing System (ASOS) User's Guide*.

Remer, L. A., D. Tanré, Y. J. Kaufman, R. Levy, and S. Mattoo. 2009. *Algorithm for remote sensing of tropospheric aerosol from MODIS for Collection 005: Revision 2*. Goddard Space Flight Center, Greenbelt, MD: National Aeronautics and Space Administration.

Remer, L. A., Y. J. Kaufman, D. Tanré, S. Mattoo, D. A. Chu, J. V. Martins, R. -R. Li, C. Ichoku, R. C. Levy, R. G. Kleidman, T. F. Eck, E. Vermote, and B. N. Holben. 2005. "The MODIS Aerosol Algorithm, Products, and Validation." *J. Atmos. Sci.* 62 (4)**:** 947-973.

Retalis, A., D. G. Hadjimitsis, S. Michaelides, F. Tymvios, N. Chrysoulakis, C. R. I. Clayton, and K. Themistocleous. 2010. "Comparison of aerosol optical thickness with in situ visibility data over Cyprus." *Nat. Hazards Earth Syst. Sci.* 10: 421-428.

Richards, L. W., T. S. Dye, M. Arthur, and M. S. Byars,.1996. *Analysis of ASOS Data for Visibility Purposes, Final Report*. San Rafael, CA: Systems Applications International, Inc.

Rienecker, M. M., M. J. Suarez, R. Todling, J. Bacmeister, L. Takacs, H. –C. Liu, W. Gu, et al. 2008. "The GEOS-5 Data Assimilation System--Documentation of Version 5.0.1, 5.1.0, and 5.2.0." *NASA Technical Report Series on Global Modeling and Data Assimilation* 27 (December 30): 1–118.

Rienecker, M. M., and Coauthors. 2011. "MERRA: NASA's Modern-Era for Research and Applications." *J. Climate.* 24 (14): 3624-3648. doi: http://dx.doi.org/10.1175/JCLI-D-11-00015.1.

Schaap, M., A. Apituley, R. M. A. Timmermans, R. B. A. Koelemeijer, and G. De Leeuw. 2009. "Exploring the relation between aerosol optical depth and $PM_{2.5}$ at Cabauw, the Netherlands." *Atmos. Chem. Phys.* 9: 909-925.

Takemura, T., T. Nakajima, O. Dubovik, B. N. Holben, and S. Kinne. 2002. "Single-Scattering Albedo and Radiative Forcing of Various Aerosol Species with a Global Three-Dimensional Model." *J. Climate.* 15 (4): 333-352.

Tang, I.N., and H.R. Munkelwitz. 1994. "Water activities, densities, and refractive indices of aqueous sulfates and sodium nitrate droplets of atmosphere importance." *J. Geophys. Res.*, 99 (D9): 18,801-18,808.

Tanré, D., M. Herman, and Y. J. Kaufman. 1996. "Information on aerosol size distribution contained in solar reflected spectral radiances." *J. Geophys. Res.* 101 (D14): 19,043-19,060.

Tanré, D., Y. J. Kaufman, M. Herman, and S. Mattoo. 1997. "Remote sensing of aerosol properties over oceans using the MODIS/EOS spectal radiances." *J. Geophys. Res.* 102 (D14): 16,971-16,988.

Taylor, K. E. 2001. "Summarizing multiple aspects of model performance in a single diagram." *J. Geophys. Res.* 106 (D7): 7183-7192.

Tsai, T. –C., Y. –J. Jeng, D. A. Chu, J. –P. Chen, S. –C. Chang. 2011. "Analysis of the relationship between MODIS aerosol optical depth and particulate matter from 2006 to 2008." *Atmos. Environ.* 45 (27): 4777-4788. doi: 10.1016/j.atmosenv.2009.10.006.

Tsay, S.-C., G. L. Stephens, and T. J. Greenwald. 1991. "An investigation of aerosol microstructure on visual air quality." *Atmos. Enviro*n. 25 (5): 1039-1053.

Van Donkelaar, A., R. V. Martin, and R. J. Park. 2006. "Estimating ground-level $PM_{2.5}$ using aerosol optical depth determined from satellite remote sensing." *J. Geophys. Res.* 111: D21201. doi:10.1029/2005JD006996.

Van Donkelaar, A., R. V. Martin, M. Brauer, R. Kahn, R. Levy, C. Verduzco, and P. J. Villeneuve. 2010. "Global Estimates of Ambient Fine Particulate Matter Concentrations from Satellite-Based Aerosol Optical Depth: Development and Application." 2010. *Environ. Health. Perspec.* 118 (6): 847-855.

Vermote, E. F., S. Vibert, H. Kilcoyne, D. Hoyt, and T. Zhao. 2002. *Suspended Matter: Visible/Infrared Imager/Radiometer Suite algorithm theoretical basis document.*

Maryland: Raytheon Systems Company, Information Technology and Scientific Services.

Wang, J., and S. A. Christopher. 2003. "Intercomparison between satellite-derived aerosol optical thickness and $PM_{2.5}$ mass: Implications for air quality studies." *Geophys Res. Lett.* 30 (21): 2095. doi: 10.1029/2003GL018174.

Wang, J., A. A. Hoffmann, R. Park, D. J. Jacob, and S. T. Martin. 2008, "Global distribution of solid and aqueous sulfate aerosols: effect of the hysteresis of particle phase transitions", *J. Geophys. Res.*, 113: D11206.

Wang, K., R. E. Dickinson, and S. Liang. 2009. "Clear Sky Visibility Has Decreased over Land Globally from 1973 to 2007." *Science.* 323: 1468-1479.

Watson, J. G., E. Fujita, J. C. Chow, and B. Zielinska. 1998. *Northern Front Range Air Quality Study Final Report* Colorado State University: Office of the Vice President for Research and Information Technology.

World Meteorological Organization. 2008. *Guide to Meteorological Instruments and Methods of Observation (seventh edition). WMO-No. 8.* Geneva, Switzerland.

Zhang, H., R. M. Hoff, and J. A. Engel-Cox. 2009. "The Relation between Moderate Resolution Imaging Spectroradiometer (MODIS) Aerosol Optical Depth and PM2.5 over the United States: A Geographical Comparison by U.S. Environmental Protection Agency Regions." *J. Air & Waste Manage. Assoc.* 59 (11): 1358-1369.

Tables

Table 1. Percentage of data lost to each step of quality control for individual ASOS stations for the year 2005. Stations with 3 visibility sensors are marked with an asterisk*. Letters in first column correspond to the Taylor Diagrams in Fig. 7.

Station		QC 1 (%)	QC 2 (%)	QC 3 (%)	QC 4 (%)	TOTAL (%)
A	**KATL**	0.9	9.6	1.3	66.7	70.1
B	**KBDR**	10.5	8.1	0.4	60.4	67.3
C	**KBKW**	9.4	13.2	1.1	95.8	97.0
D	**KBNA**	10.9	2.5	0.7	27.4	37.0
F	**KBWI**	8.2	6.4	0.3	24.5	34.0
G	**KCLT**	7.0	9.9	0.5	25.1	34.3
	KCMH	7.7	6.9	0.5	58.6	60.8
H	**KCVG**	8.9	6.9	0.6	57.4	61.5
I	**KDCA**	11.0	16.7	0.4	10.3	32.7
	KDTW	27.7	11.9	0.5	85.2	88.9
	KERI	18.0	58.7	9.4	72.8	89.0
J	**KEWR**	3.0	6.5	0.9	26.9	32.8
K	**KGRR**	15.7	10.7	0.8	65.5	69.3
L	**KISP**	27.3	37.7	0.7	45.8	74.8
	KMDW	24.3	10.9	1.0	85.2	86.1
N	**KMEM**	6.2	1.6	0.4	43.1	45.1
O	**KMKE**	20.6	5.9	0.6	62.5	74.8
P	**KMKG**	10.1	11.4	2.4	56.2	64.0
	KORD	20.8	11.3	0.9	57.3	69.1
	KORF	15.5	16.2	0.5	99.4	99.9
Q	**KPIT**	29.3	30.2	1.4	57.6	71.6
R	**KPVD**	18.3	11.5	0.4	23.9	43.1
S	**KPWM**	8.0	61.5	0.6	23.7	70.4
T	**KRDU**	1.5	12.6	1.4	26.2	34.0
U	**KSYR**	32.2	6.2	1.1	47.1	70.7
	KBDL*	27.3	15.3	15.3	58.0	76.7
E	**KBOS***	27.1	8.3	1.1	62.1	76.5
	KCLE*	1.5	1.4	0.8	70.9	71.6
L	**KIAD***	15.1	5.9	1.7	88.1	92.2
	KJFK*	7.6	5.1	0.8	95.7	96.3
M	**KLGA***	21.0	5.8	0.5	75.4	78.6
	KPHL*	12.6	6.2	3.2	66.0	70.9
All Station Average:		14.5	13.5	1.2	56.9	66.9
2 Sensor Average:		14.1	15.4	1.1	52.2	63.1
3 Sensor Average:		16.0	6.9	1.4	73.7	80.4

Figures

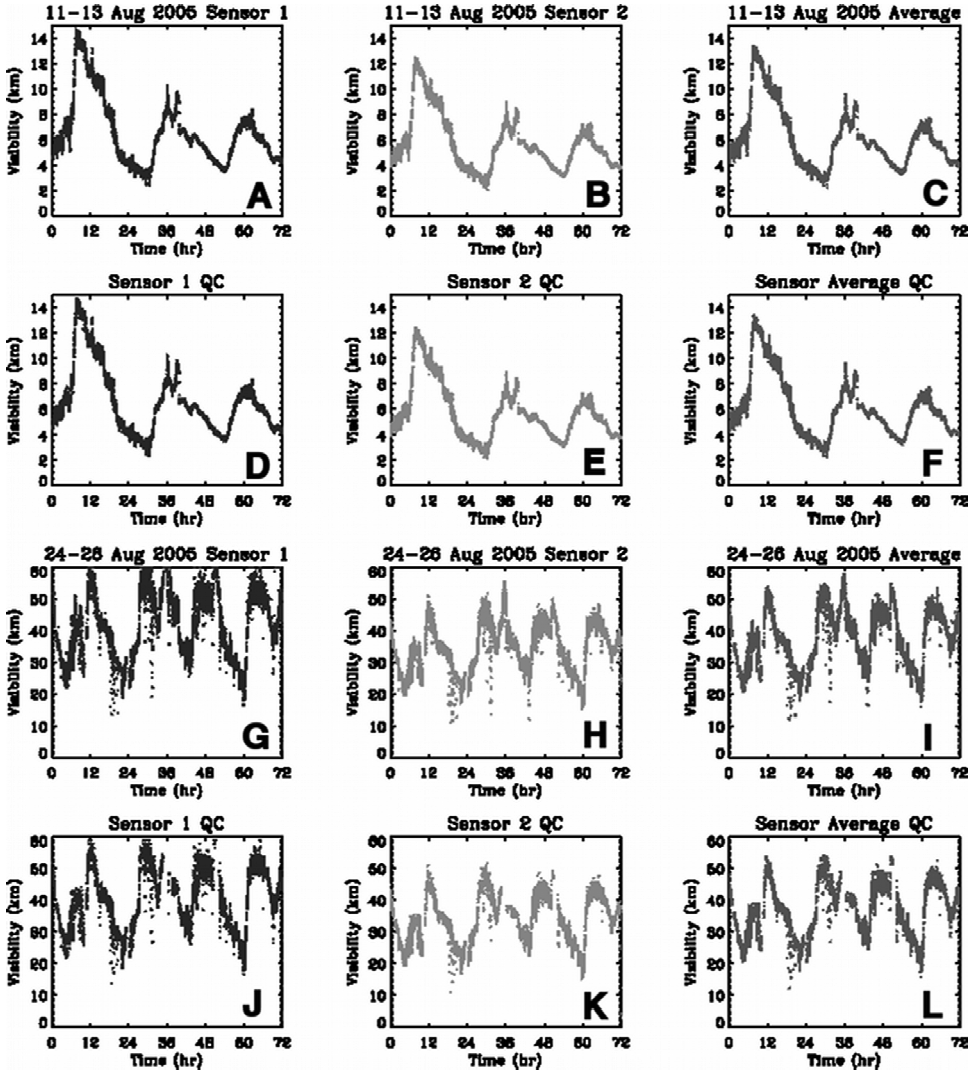

Figure 1. Time series of ASOS visibility data at Baltimore/Washington International Thurgood Marshall Airport (KBWI) for (A-F) 11-13 August 2005 and (G-L) 24-26 August 2005 before and after quality control. (A, D, G, and J) Time series for the first visibility sensor located at KBWI. (B, E, H, and K) Time series for the second visibility sensor located at KBWI. (C, F, I, and L) Time series average for both sensors located at KBWI. Time shown is in Local Time (EST).

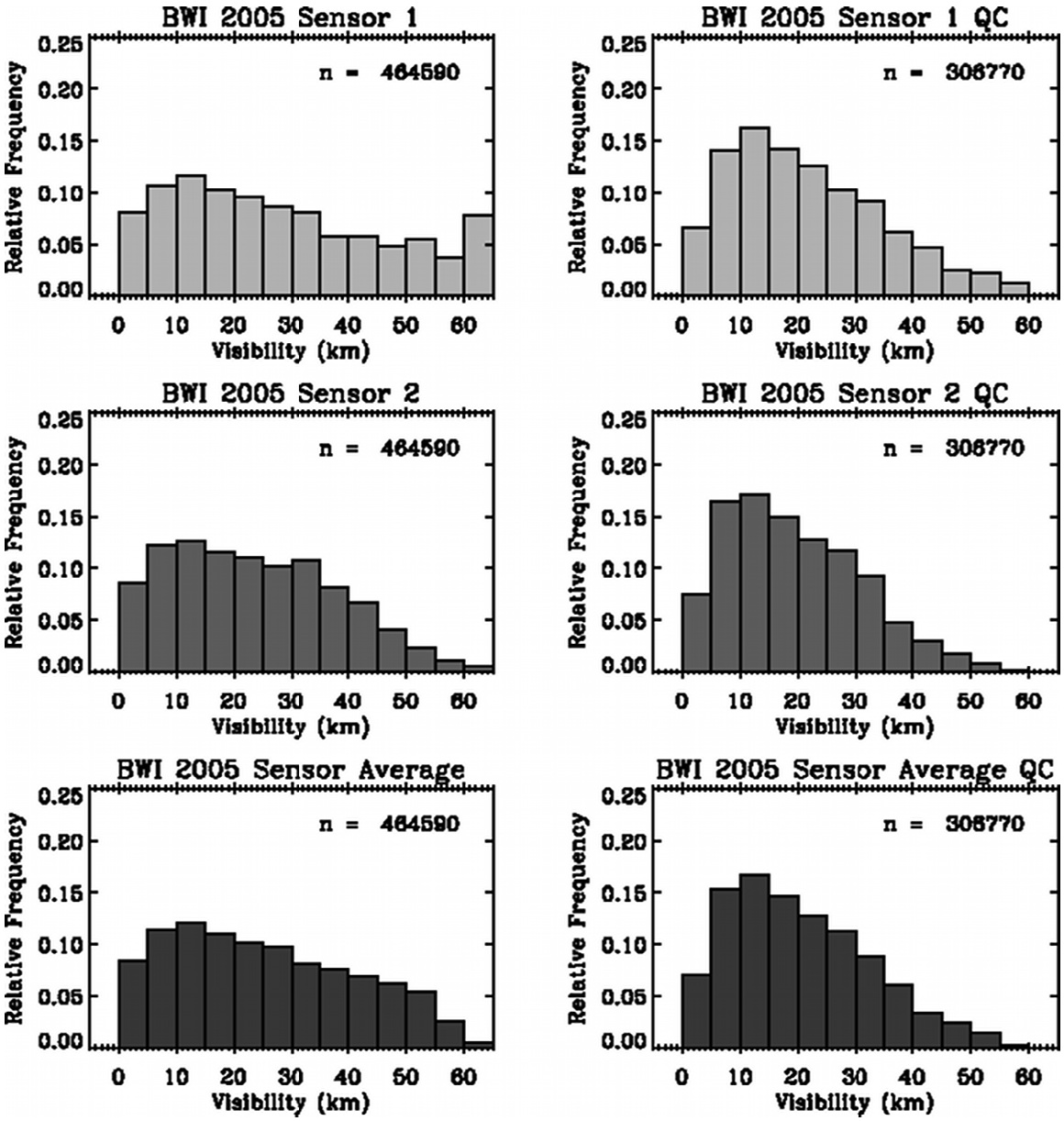

Figure 2. Relative frequency histograms of ASOS visibility data at KBWI for 2005 before and after quality control.

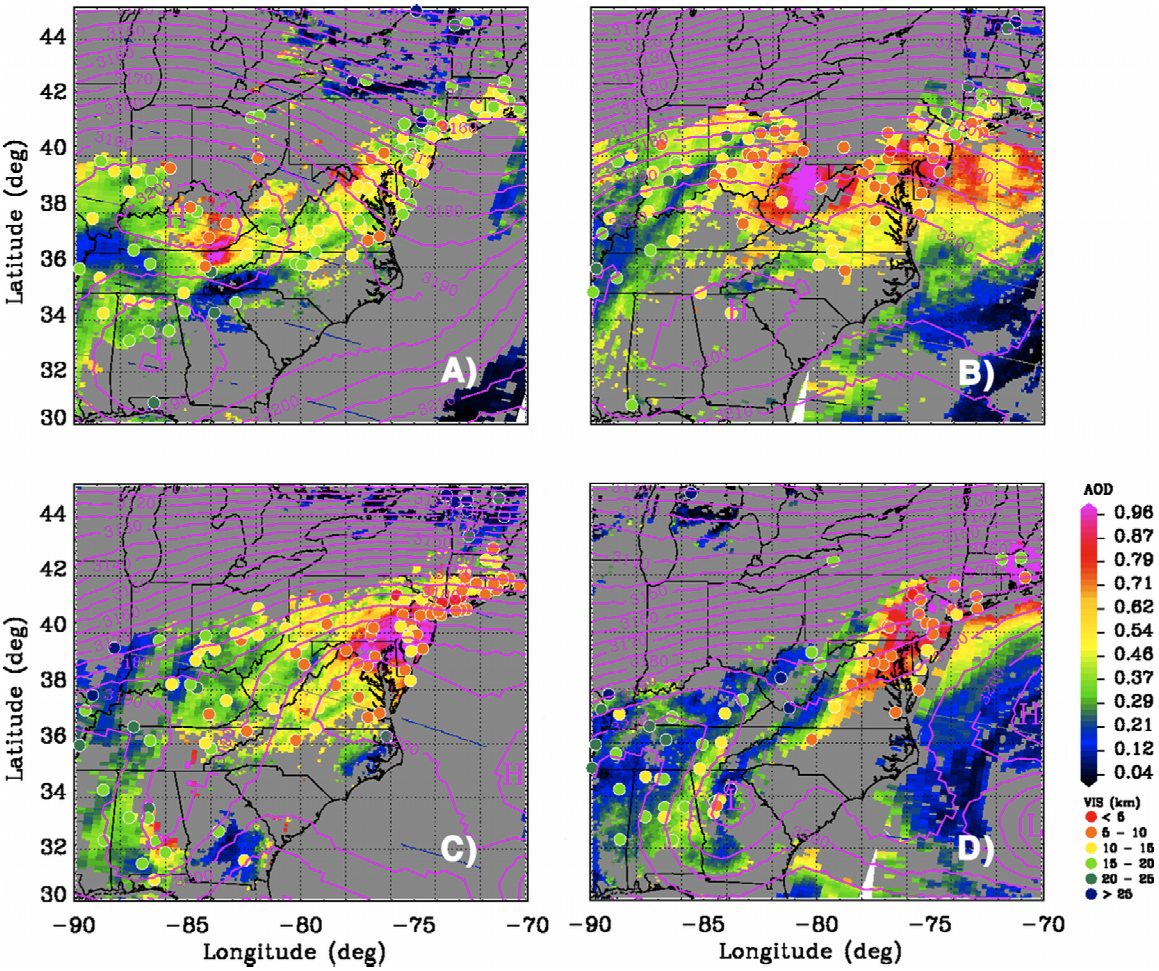

Figure 3. Map of MODIS AOD and ASOS visibility for (a) 11 August 2005, (b) 12 August 2005, (c) 13 August 2005, and (d) 14 August 2005. ASOS visibility is denoted by circles. Pink lines represent North American Regional Reanalysis (NARR) 700-hPa geopotential heights. Gray coloring represents cloud.

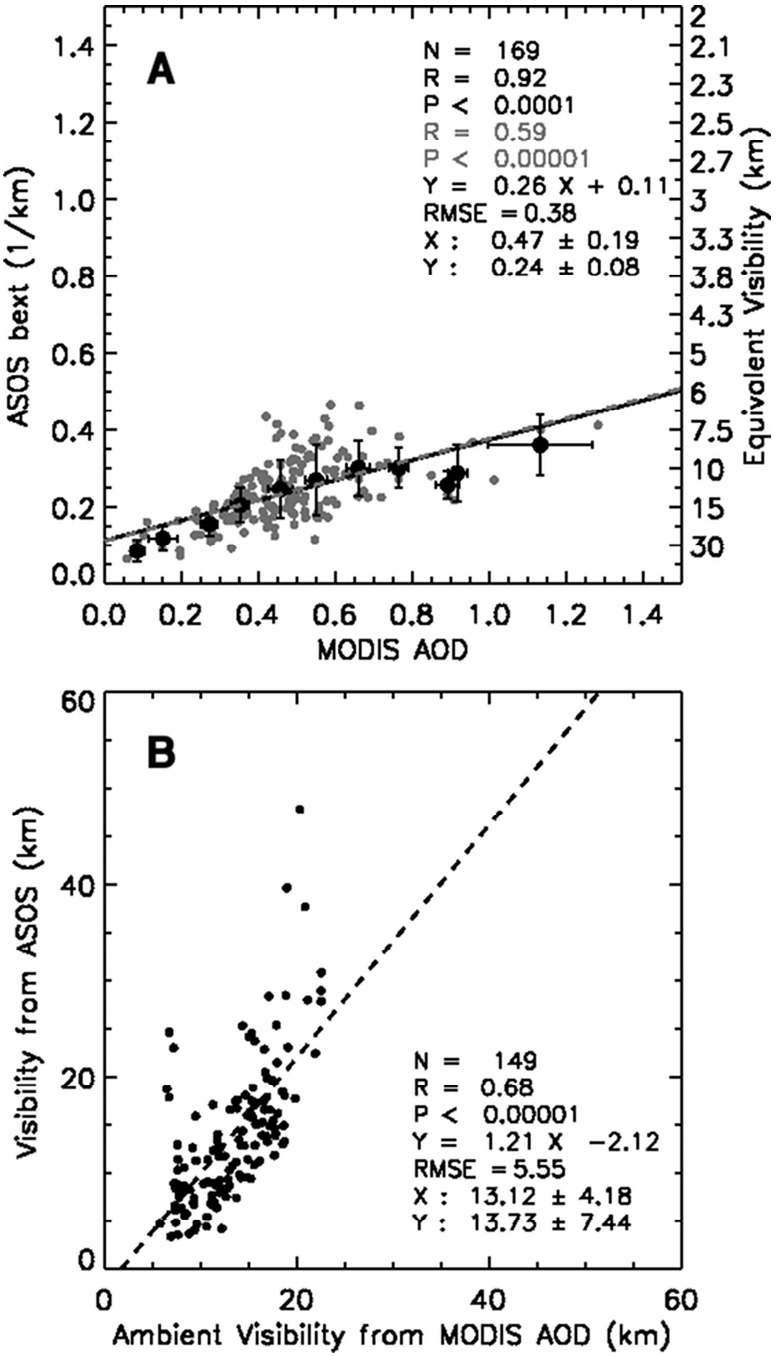

Figure 4. (a) Correlation plot of MODIS AOD versus ASOS b_{ext} for 11-12 August 2005. Binned data are shown in black. (b) Correlation plot of modeled ambient visibility from MODIS AOD versus visibility from ASOS for 13-14 August 2005.

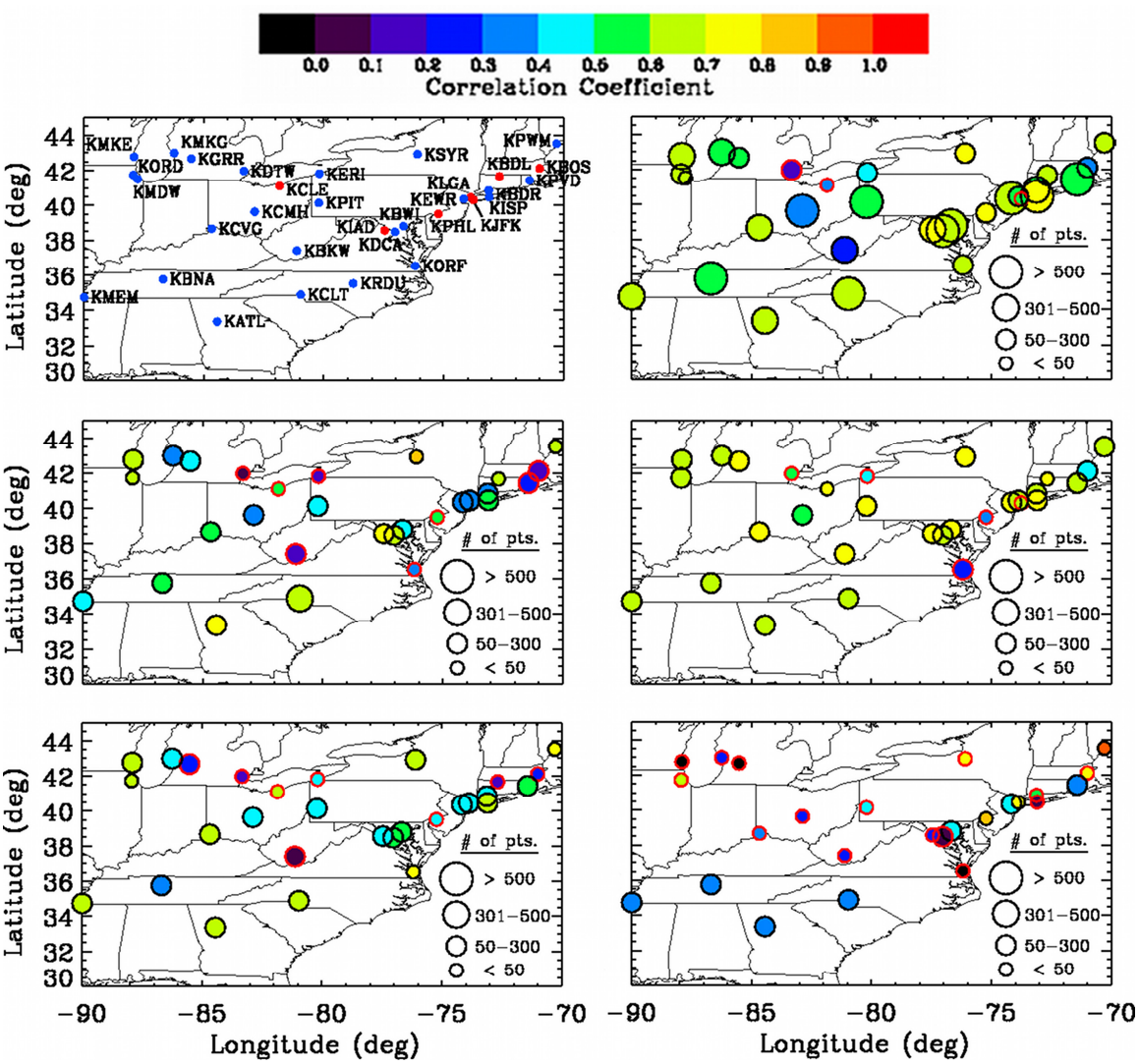

Figure 5. (a) Map of ASOS stations used in long-term analysis. Blue circle stations have two visibility sensors. Red circle stations have three visibility sensors. (b) Map of the correlation between ASOS b_{ext} and MODIS AOD for the stations shown in (a) for the years 2000-2011. (c) Similar to (b) but for spring (MAM). (d) Similar to (b) but for summer (JJA). (e) Similar to (b) but for fall (SON). (f) Similar to (b) but for winter (DJF). In (b-f), circles outlined in red are not significant data.

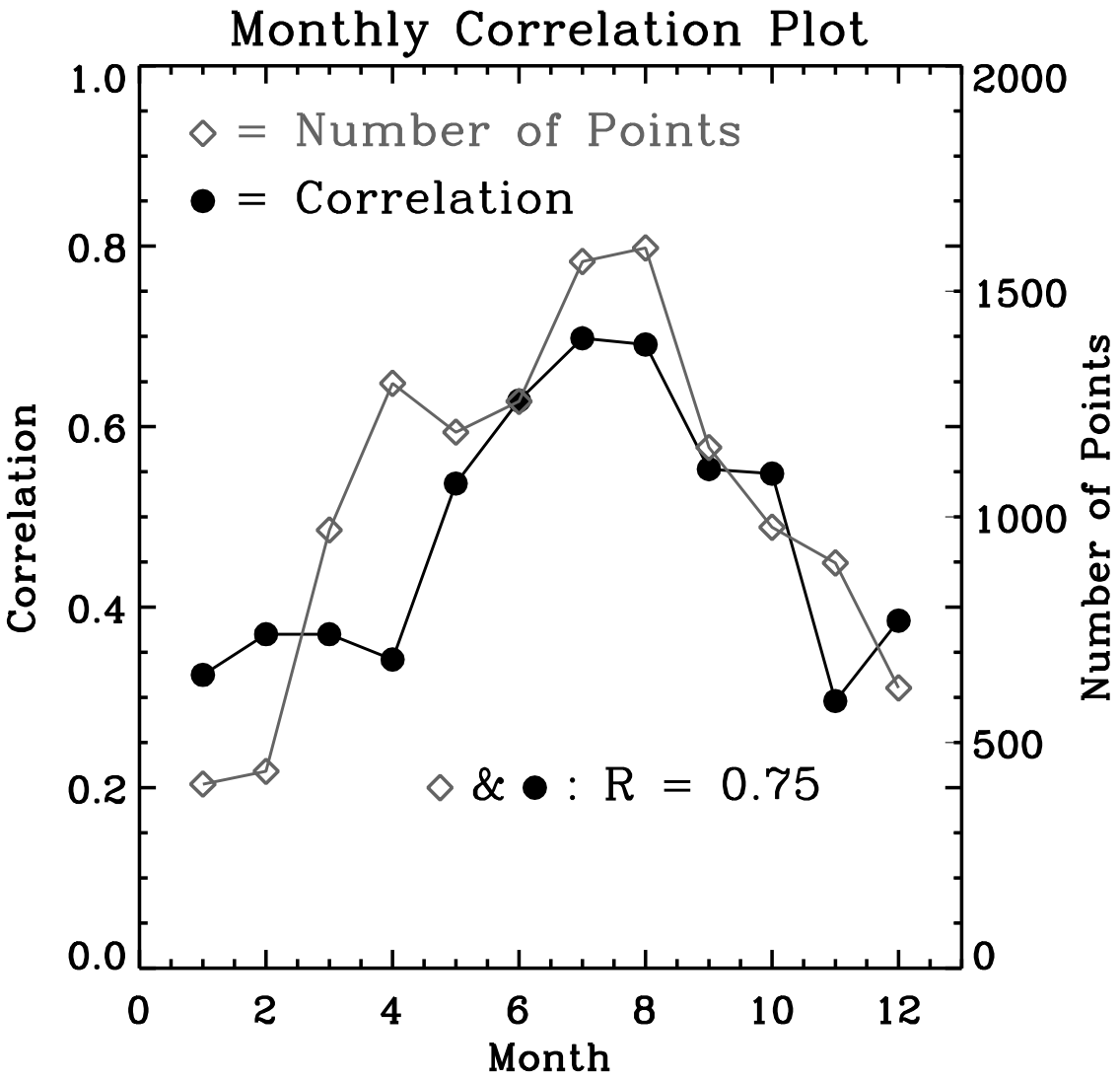

Figure 6. Monthly correlation plot of ASOS σ_{ext} versus MODIS AOD for the years 2000-2011 shown by black circles. Number of points used in monthly correlation calculation shown by gray diamonds.

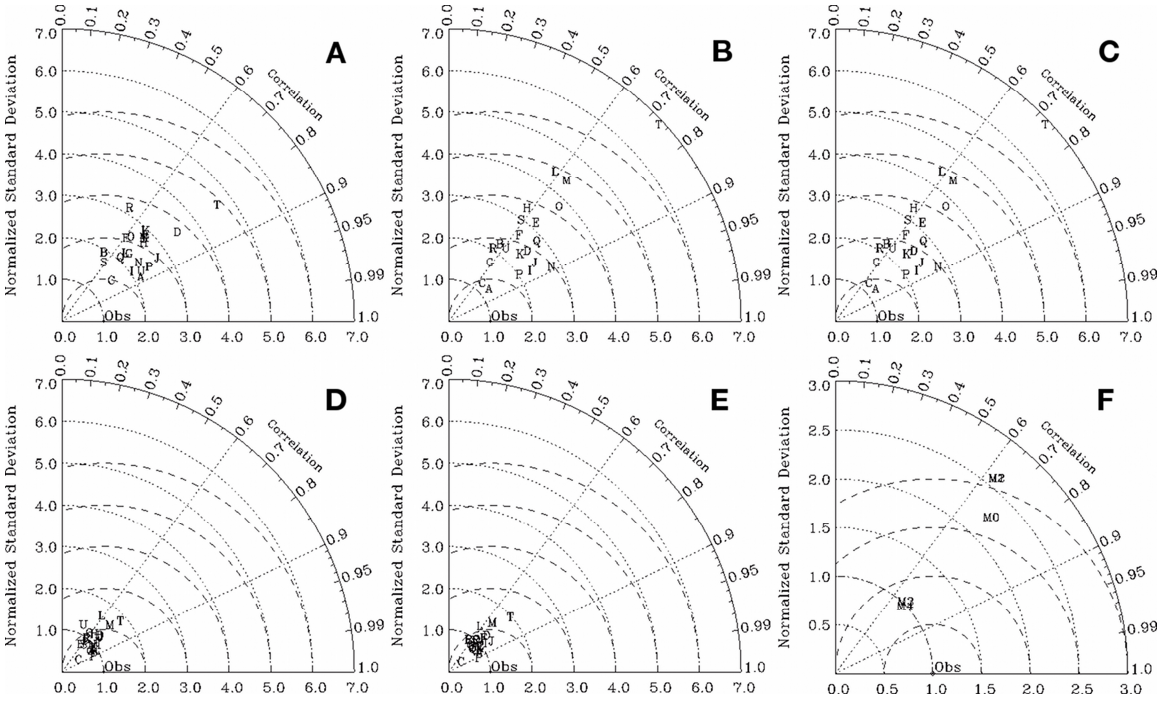

Figure 7. Taylor Diagram showing correlation, normalized standard deviation, and normalized RMSD for 22 ASOS stations using (a) M0, (b) M1, (c) M2, (d) M3, and (e) M4. (f) Taylor Diagram comparing all 5 methods using all 32 ASOS stations. Note scale is different for (f). Key for diagrams (a) – (e) is located in Table 1.

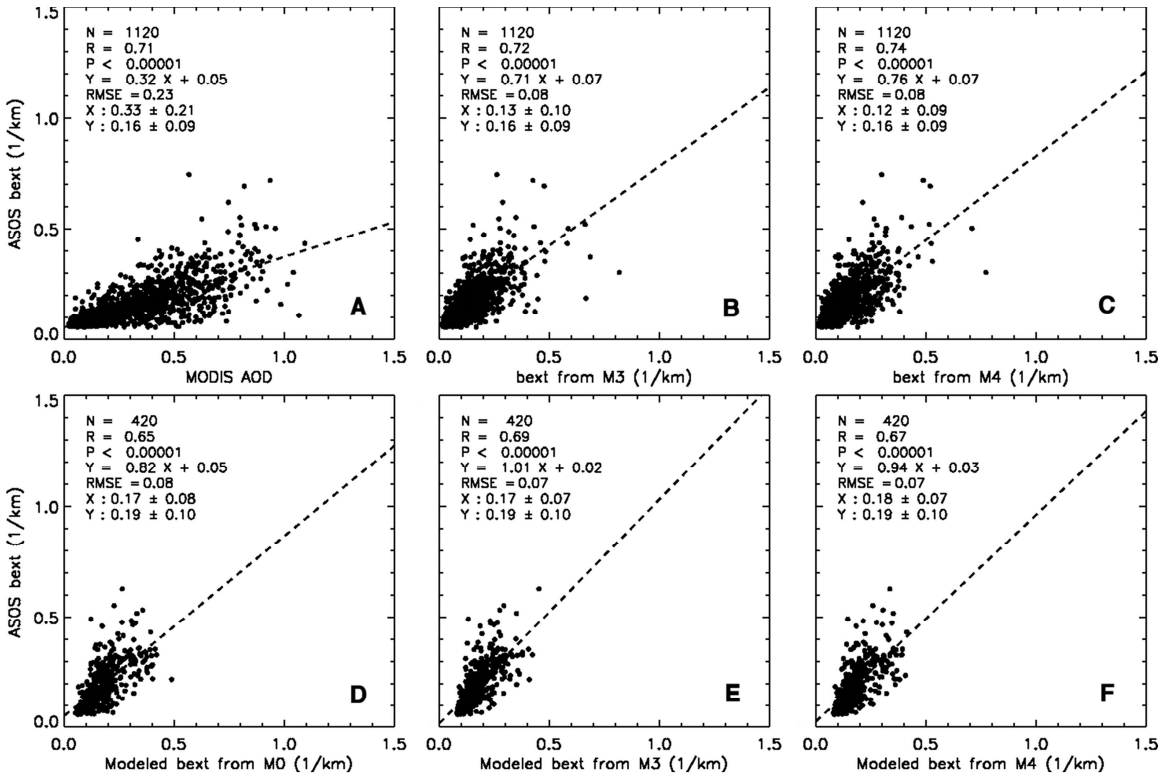

Figure 8. Correlation plots of (a) MODIS AOD versus ASOS b_{ext} for 2003-2004 and 2006 (M0), (b) b_{ext} from M3 versus ASOS b_{ext} for 2003-2004 and 2006, (c) b_{ext} from M4 versus ASOS b_{ext} for 2003-2004 and 2006, (d) modeled b_{ext} from Mod0 versus ASOS b_{ext} for 2005, (e) modeled b_{ext} from Mod3 versus ASOS b_{ext} for 2005, and (f) modeled b_{ext} from Mod4 versus ASOS b_{ext} for 2005.

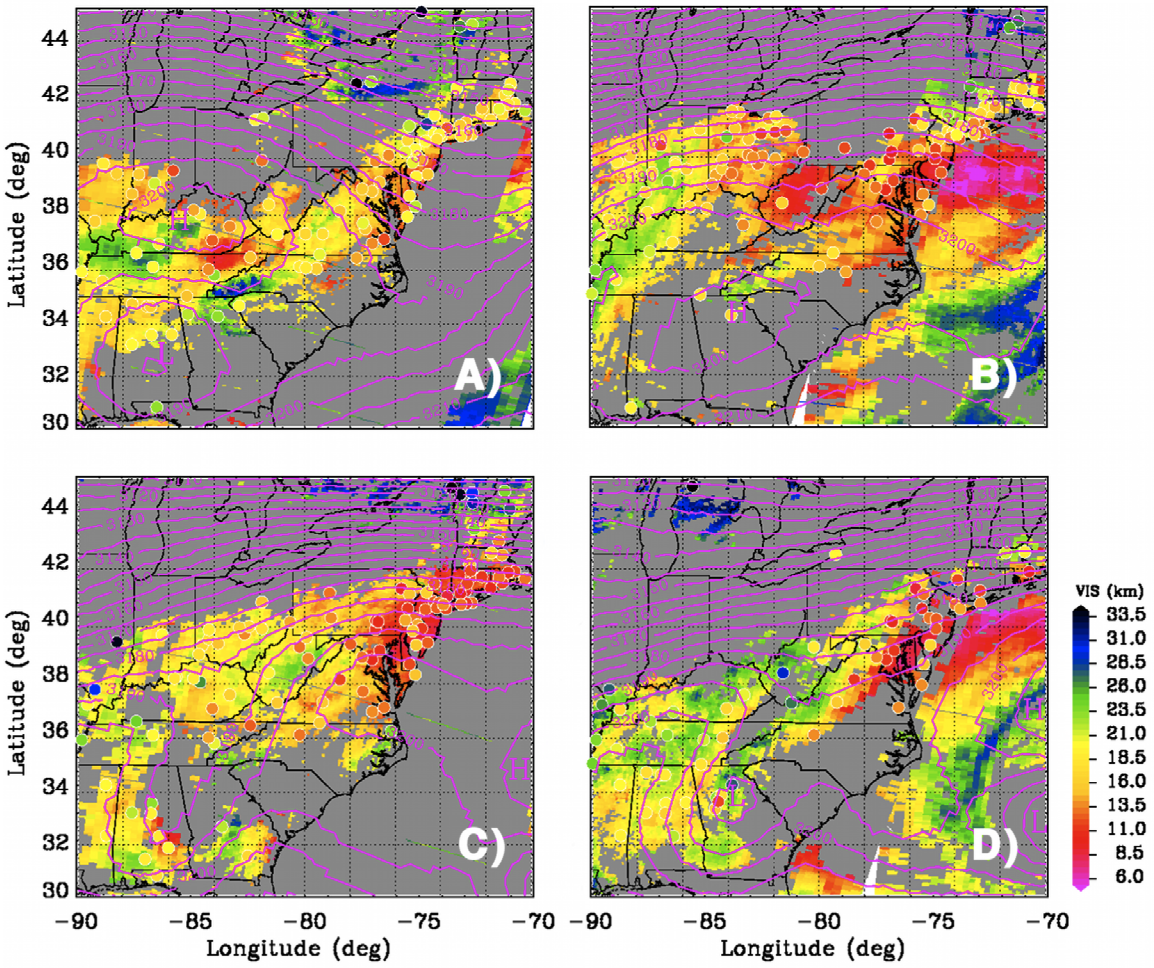

Figure 9. Map of modeled visibility from Mod3 and ASOS visibility for (a) 11 August 2005, (b) 12 August 2005, (c) 13 August 2005, and (d) 14 August 2005. ASOS visibility is denoted by circles. Pink lines represent North American Regional Reanalysis (NARR) 700-hPa geopotential heights. Gray coloring represents cloud.

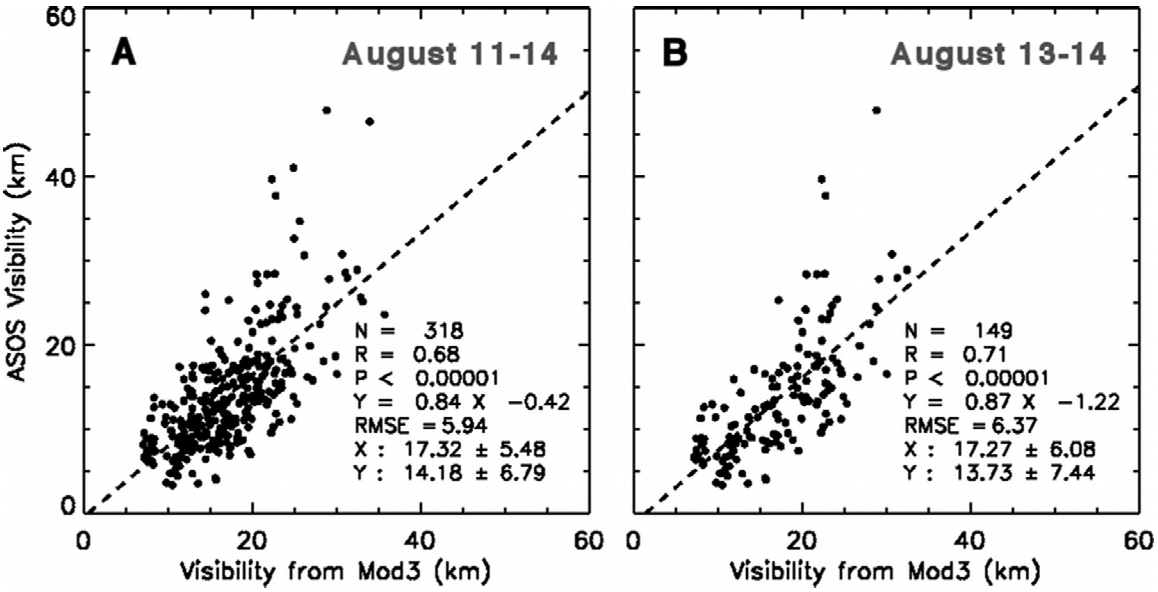

Figure 10. Correlation plots of modeled visibility from Mod3 versus ASOS visibility for (a) 11-14 August 2005, and (b) 13-14 August 2005.